Destruction of high-n (n~300) Rydberg atoms in Rydberg-Rydberg collisions

G. Fields, F. B. Dunning, S. Yoshida, and J. Burgdörfer

Phys. Rev. A **99**, 022710 — Published 26 February 2019

DOI: 10.1103/PhysRevA.99.022710

Destruction of high-n, $n \sim 300$, Rydberg atoms in Rydberg-Rydberg collisions

G. Fields,[1] F. B. Dunning,[1] S. Yoshida,[2] and J. Burgdörfer[2]

[1]*Department of Physics and Astronomy,*

Rice University, Houston, TX 77005-1892, USA

[2]*Institute for Theoretical Physics, Vienna University of Technology Vienna, Austria, EU*

Abstract

The destruction of high-n, $n \sim 300$, strontium atoms contained in a hot atomic beam through Rydberg-Rydberg collisions is examined. The Rydberg atoms are initially created, under blockade conditions, in a localized volume and their subsequent motions lead to creation of a string of Rydberg atoms. The Rydberg atoms, however, are formed with a thermal distribution of velocities resulting in Rydberg-Rydberg collisions which lead to their destruction. The experimental data are interpreted using classical trajectory Monte Carlo techniques that simulate the excitation of the Rydberg atoms together with their subsequent motions. Using calculated collisional ionization cross sections and blockade radii, the model yields results in good agreement with experiment. The results highlight the important role collisional destruction can play when attempting to study (long-range) Rydberg-Rydberg interactions in a hot atomic beam.

I. INTRODUCTION

Because of their strong mutual long-range interactions, Rydberg atoms provide an attractive vehicle with which to explore the behavior of strongly-interacting few- and many-body systems [1–3]. The strength of their interactions can be controlled by varying the atomic separations and the atomic states created; in particular their principal quantum numbers n and their angular momenta [4–9]. Rydberg-Rydberg interactions have been exploited in the development of quantum gates [10–12] and in manipulating the interactions between atoms confined in an optical lattice [13, 14]. In addition, the interaction between "ground-state" atoms can be controlled by dressing the atoms with radiation tuned near resonance with the transition to a Rydberg state which introduces a small amount of Rydberg character into the atomic wave function [15]. One challenge in working with high-n atoms is that due to their large physical size and weak binding they can be readily ionized by collisions, especially by collisions with other Rydberg atoms. Such ionization has been observed in ultracold gases of atoms and is known to initiate the formation of ultracold plasmas [16–20]. In ultracold gases Rydberg-Rydberg collisions result from the weak accelerations induced by their van der Waals attraction and, although the rate of collisions is typically small, the collisional cross sections can be large due to the long range nature of their interactions [21–23]. In contrast, in a hot atomic beam the collision energies dominate over the energies associated with van der Waals interactions and the initial impact parameter determines the probability for collisional ionization.

Recent work [24, 25] in this laboratory has shown that even at very-high-n, $n \geq 300$, it is possible to observe dipole blockade in a hot strontium atomic beam by using tightly-focused laser beams to create a localized excitation volume and that the blockade radius is large, $\sim 100\mu$m. Such blockade can be exploited to generate a string of Rydberg atoms (see Fig. 1) whose initial separations d are governed principally by the time it takes a Rydberg atom, once created, to travel sufficiently far from the excitation volume that another Rydberg atom can be excited. In a hot atomic beam, however, Rydberg atoms having a thermal distribution of velocities are formed. In consequence, although the Rydberg atoms are initially created with large approximately-equal spacings, their separations evolve in time leading to collisions which can result in state changing and in Rydberg atom destruction. In the present work we examine the collisional destruction of high-n, $n \sim 300$, strontium

n^1F_3 Rydberg atoms excited in a hot atomic beam by monitoring the time evolution of the high-n population.

When the relative velocity of the collision partners is much smaller than the average velocity of their Rydberg electrons, Penning ionization [26, 27]

$$\mathrm{Sr}(n) + \mathrm{Sr}(n) \rightarrow \mathrm{Sr}(n') + \mathrm{Sr}^+ + \mathrm{e}^- \tag{1}$$

is expected to be the dominant Rydberg atom destruction process. The slow relative motion allows the interaction energy to evolve adiabatically and only minimal energy exchange between nuclear and electronic motions occurs. Consequently, conservation of electronic energy requires that the neutral product be left in a final state with $n' < n/\sqrt{2}$, i.e., the final state of the atom must have at least twice the binding energy of the initial state. For collisions of high-n Rydberg atoms the density of states around the final state is typically high and, therefore, a classical analysis is valid for the study of collisional ionization [21, 28]. However, for low-n Rydberg atoms in ultracold gases the avoided crossings between adiabatic quasi-molecular levels may become dynamically relevant whereupon the ionization dynamics must be analyzed quantum mechanically [23]. In the present experimental study the typical relative collision velocities, ~ 200 m s^{-1}, are much smaller than the average velocity of the Rydberg electron (~ 7300 m s^{-1} at $n \sim 300$) and Penning ionization is responsible for the bulk of the Rydberg loss. The relative velocity, however, is still well above those at which quantum effects become important.

The use of Rydberg atoms in extremely high-n ($n \sim 300$) levels allows the experimental data to be analyzed using classical trajectory Monte Carlo (CTMC) calculations to simulate both the excitation of the Rydberg atoms and their subsequent motion in the beam. The model requires as input parameters the blockade radius and the ionization cross section. We employ the blockade radius that was derived previously for $n \sim 300$ $^1\mathrm{F}_3$ states by solving the time-independent Schrödinger equation [25]. The collisional ionization cross section is calculated using a CTMC code [28]. The model predictions are in good agreement with the experimental results. The data point to large collisional loss cross sections, $\sigma_{\mathrm{ion}} \sim 1-2\times10^{-6}$ cm^2, which are on the order of those expected for "hard sphere" collisions, i.e., $\sigma \sim 4\pi R_n^2$ where $R_n \sim 2n^2$ is the atomic radius. (Unless otherwise specified, atomic units are used throughout.)

II. EXPERIMENTAL METHOD

In the present work, strontium Rydberg atoms are created in a tightly-collimated beam through laser-induced multiphoton excitation. The (crossed) laser beams employed are tightly focused to define a small excitation volume whose linear dimensions, $\sim 50\mu$m, are less than the blockade radius, $R_b \sim 100\mu$m at $n \sim 300$ [25]. Production of a Rydberg atom in this volume thus suppresses further excitation until the atom has traveled $\sim 100\mu$m in the beam direction which, given the mean velocity of atoms in the strontium beam, $\bar{v} \sim 4 \times 10^2$ m s^{-1}, typically requires ~ 250 ns. Thus, when using high laser powers for which the photo-excitation rate is sufficient that excitation of an additional Rydberg atom occurs quickly once a previously-excited atom has moved more than a blockade radius, a string of Rydberg atoms can be produced with approximately equal initial separations (but a distribution of initial velocities). Here laser pulse widths of $\sim 10\mu$s are employed which allows production of a sizable number (typically up to ~ 40) Rydberg atoms allowing the effects of collisions to be observed.

The present apparatus is shown in Fig. 2 and has been described in detail previously [25]. Briefly, strontium n^1F_3 Rydberg atoms (quantum defect ~ 0.09) are created in near-zero electric field at the center of an interaction region defined by three pairs of copper electrodes. (Stray fields in the excitation volume are locally reduced to $\lesssim 10\mu$V cm^{-1} by application of small offset voltages to these electrodes.) The three-photon Rydberg excitation scheme employed, $5s^2\ {}^1S_0 \rightarrow 5s5p\ {}^1P_1 \rightarrow 5s5d\ {}^1D_2 \rightarrow 5snf\ {}^1F_3$, is illustrated in the inset in Fig. 2 and requires radiation at 461, 767, and 893 nm that is provided by diode laser systems whose wavelengths are stabilized using Fabry-Perot transfer cavities locked to a polarization-stabilized HeNe laser. The use of three-photon excitation has the advantage that sizable laser powers, $\sim$ 1W, are available to drive the final transition to the Rydberg state. (The decay rates associated with $5s5p\ {}^1P_1 \rightarrow 5s4d\ {}^1D_2$ and $5s5d\ {}^1D_2 \rightarrow 5s6p\ {}^1P_1$ transitions are small, $\sim 3 \times 10^3$ and 9×10^3 s^{-1}, respectively, and the population of such states is unimportant on the time scale of the present laser pulses.) The crossed 767 and 893 nm beams are focused to $1/e^2$ diameters of ~ 50 and 70μm, respectively, resulting in a strongly-localized excitation volume of $\sim 10^{-7}$ cm^3 that typically contains tens to hundreds of ground state atoms.

Measurements are conducted in a pulsed mode. The output of the 461 nm laser, which is not focused, is chopped into a series of pulses with a pulse repetition frequency of $\sim$ 5-

10 kHz and duration $\sim 10\mu$s using an acousto-optic modulator. (The other laser beams remain on at all times.) The evolution of the (high-n) Rydberg population during and after the laser pulses is determined by selective field ionization (SFI) which is accomplished by generating an electric field ramp in the experimental volume by applying a linearly-increasing voltage ramp to the lower electrode. In recording data for laser pulses shorter than 10 microseconds the laser was turned off after the selected pulse duration and the ionizing ramp applied immediately thereafter. The Rydberg atoms were typically ionized within 1 to 1.5 microseconds following the start of the voltage ramp thereby allowing little time for collisions during the ramp. The maximum height of the voltage ramp that can be applied is limited by the requirement that it returns very close to zero prior to the next laser pulse, i.e., within $\sim 100\mu$s of the end of the ramp. This limits the strength of the SFI field that can be applied and which is only sufficient to ionize states with $n \gtrsim 260 - 270$. In consequence, Rydberg states populated through Penning ionization (with $n' \sim n/\sqrt{2}$) are not directly detected and contribute to the measured loss of parent high-n atoms. Product electrons exit the interaction region through a pair of 80% transparent fine mesh grids and enter a cylindrical lens after which they pass through a further grid and strike the dual-microchannel-plate (MCP) detector whose output is fed to a multichannel scaler (MCS) to obtain the electron arrival time distribution at the MCP. Measurements of the time during the ramp at which ionization occurs can be used to determine the ionizing field.

In measuring the number of Rydberg atoms present in the experimental volume two factors are important: the probability that when an electron has been produced by field ionization it is collected and impacts the MCP detector, and the probability that upon arrival at the detector it produces a signal count. To address the electron collection issue a series of simulations of electron trajectories through the apparatus were undertaken using SIMION for a variety of operating conditions. These simulations showed that electrons produced by field ionization of Rydberg atoms that have traveled up to ~ 3 cm from their points of formation are efficiently collected and strike the detector. Given that the fastest atoms in the ground-state atom beam have velocities, v, of $\sim 10^3$ m s^{-1}, this limits the time over which collisional loss can be studied to $\lesssim 30\mu$s. Application of small offset biases such as used to cancel the electric field in the excitation volume was seen to have only a minimal effect on the overall collection efficiency.

The electron detection efficiency of the MCPs could not be determined directly. Whereas

new MCPs can yield detection efficiencies as high as 0.8 [29], we noted that significantly higher voltages had to be applied to the MCPs than when new to saturate the observed count rates pointing to their degradation over time. Here we assume a detection efficiency of ~ 0.5 which, when the effects of grid transparency are included, results in an estimated overall electron detection efficiency, η, of ~ 0.3. To validate this choice, Rydberg atom number distributions were recorded under conditions similar to those used in our earlier studies of Rydberg blockade [25] and the corresponding Mandel Q parameters determined. The value of the Q parameter scales as η and the results, when corrected using $\eta = 0.3$, yielded values in good agreement both with the earlier measurements and with theoretical predictions.

III. SIMULATION OF COLLISIONS BETWEEN RYDBERG ATOMS

The effect of atomic motion and blockade on the excitation of Rydberg atoms in a hot atomic beam has been studied using a rate equation approach which reproduced well the experimental observations [25]. In this earlier work, however, the duration of the excitation laser pulse was limited to a few hundred nanoseconds. For a blockade radius of $\sim 100\mu$m and a typical relative velocity (~ 200 m s^{-1}) between Rydberg atoms the time interval between collisions is about 500 ns (see Fig. 1) and thus collisions did not play a significant role in the earlier studies. In the present work considerably longer laser pulses (~ 10 μs) are employed allowing collisions to occur. To analyze the effect of such collisions, we first calculate the ionization cross section using a classical trajectory Monte Carlo (CTMC) simulation [21, 28]. The calculated cross sections serve as input for simulations that model both the excitation and the collisional destruction of Rydberg atoms using a rate equation approach. The rate equations are solved using a Monte Carlo sampling technique.

A. Ionization cross section

The ionization dynamics in collisions between Rydberg atoms depend strongly on the collision velocity. When the collision velocity, V, is much larger than the orbital velocity of the Rydberg electron $v_n = 1/n$ (~ 7300 m s^{-1} for $n \sim 300$), the interaction of a Rydberg atom with the excited electron and core ion of a second Rydberg atom are of short duration

and can be treated impulsively. The energy transfer resulting from binary electron-electron or electron-ion collisions can lead to ionization. Such impact ionization is the dominant process at high velocities, $V > v_n$. For velocities $V < v_n$, the energy exchange between the "projectile" electron and the "target" core ion is suppressed and electron-electron collisions become dominant. In this regime the relative velocity $|\vec{v}_i - \vec{v}_j|$ between the projectile and target electrons governs the scattering process. For atomic velocities within the range $V_A < V < v_n$, the collision partners travel along constant velocity trajectories with a fixed impact parameter b. Below the critical velocity, V_A, at which the Rydberg atom-Rydberg atom interaction energy U_A becomes comparable to the collision energy, i.e., $\mu V_A^2/2 \simeq U_A$ where μ is the reduced mass, the collisional partners no longer follow constant velocity straight-line trajectories and this must be taken into account. In the present case U_A results from the dipole-dipole interaction and is given by $U_A \simeq d_1 d_2/R^3$ where the dipole moments $d_1 \sim d_2 \simeq 2n^2$. At a separation $R \sim 20$ μm (the distance for hard-sphere collisions, see below), $U_A \simeq 4$ GHz , corresponding to a collision velocity V_A of ~ 8 m s^{-1}. For even lower velocities the collision energy becomes comparable to or smaller than the energy spacings near avoided crossings between the quasi-molecular levels formed during a Rydberg-Rydberg collision. The average size of the energy separations is expected to be only a (small) fraction of the splitting between adjacent n levels, $\sim 1/n^3$, which for $n \simeq 300$ is ~ 250 MHz corresponding to a relative collision velocity $V_Q \sim 2$ m s^{-1}. Only for very low velocities $V < V_Q$ will quantum effects due to the discreteness of the quasi-molecular energy levels and diabatic passage through avoided crossings influence the ionization process. Because of the extremely high density of electronic states, $\sim n^3$, for very high ($n \simeq 300$) Rydberg atoms quantum effects are strongly suppressed and a classical approximation to the electronic dynamics is well justified. Typical relative collision velocities in the present experiment are ~ 200 m s^{-1} and are in the regime $V_A \ll V \ll v_n$. It is therefore reasonable to assume that the colliding atoms approach along constant-velocity straight-line trajectories.

We approximate the Rydberg-Rydberg collision in terms of an effective four-body Hamiltonian

$$H = \sum_{i=1}^{2} \left(\frac{P_i^2}{2M} + \frac{p_i^2}{2} \right) - \sum_{i,j=1}^{2} \frac{1}{|\vec{r}_i - \vec{R}_j|} + \frac{1}{|\vec{r}_1 - \vec{r}_2|} + \frac{1}{|\vec{R}_1 - \vec{R}_2|} \tag{2}$$

where we treat each of the colliding strontium Rydberg atoms using a single-active-electron approximation with the electron- Sr^+ core interaction replaced by a pure Coulomb inter-

action. In Eq.(2) $\vec{R}_i$ and $\vec{P}_i$ $(i = 1, 2)$ are the ion coordinates and momenta, $\vec{r}_i$ and $\vec{p}_i$ are the electron coordinates and momenta, and M is the mass of the Sr^+ ion. Initially, one of the atoms (the target) is at rest and the other atom (the projectile) is assumed to be sufficiently distant from the target that their interaction is negligibly small. Each atom is initially an $n\ ^1F_3$ state (angular momentum $L = 3$) with $n \sim 300$. The wave function of each Rydberg electron is approximated by a classical phase space distribution which is set to be a sub-ensemble of the microcanonical ensemble [30] with energy $E = -1/(2n^2)$ and restricted angular momentum $3^2 < L^2 < 4^2$. The projectile travels towards the scatterer with initial velocity $V = |\vec{V}_1 - \vec{V}_2|$ and impact parameter $b = |(1 - \mathcal{P}_V)\vec{R}|$, where $\vec{R} = \vec{R}_1 - \vec{R}_2$, $\vec{V}_i = \vec{P}_i/M$, and $\mathcal{P}_V$ the projection onto $\vec{V}$ (see Fig. 1). The time evolution of the phase space distribution for the total 4-body system (or, more precisely, for the 3-body system since the center-of-mass coordinate is separable) is followed by solving the Liouville equation associated with the Hamiltonian [Eq. (2)] using a CTMC approach [30]. After the projectile passes the target, the ionization probability $P_{\rm ion}(b, V)$ is evaluated. As an example, the ionization probability following the collision of two Rydberg atoms with $n = 306$ and $L = 3$ is plotted as a function of impact parameter and initial velocity in Fig. 3(a). For $V > V_A \sim 8$ m s^{-1} ionization is observed only for $b < 15\mu$m which is close to the limit for a hard-sphere collision, i.e., $4n^2 \simeq 20\mu$m, and for which there is a sizable overlap of the electron distributions. The velocity dependence is rather weak but with decreasing relative velocity ionization is observed to occur over a slightly more extended range in impact parameter b. For $V_Q < V < V_A$ the Rydberg-Rydberg interaction influences the motion of atoms [16–20]. Consequently, the colliding atoms follow a curved trajectory and ionization is observed for a wide range of impact parameters. Considering that the van der Waals interaction does not follow the classical scaling [25] quantum effects might influence the scattering process between Rydberg atoms and some quantum corrections might be necessary for quantitative studies. We note that in the velocity regime depicted in Fig. 3(a) the probability for double ionization, i.e. simultaneous ionization of both Rydberg electrons is negligibly small ($< 2\%$) even for the highest velocity and the smallest impact parameter confirming that Penning ionization is the dominant process. The projectile n-distribution after the collision, integrated over collision velocity, is shown in Fig. 3(b). As the impact parameter decreases and the interaction between the Rydberg electrons becomes important, energy exchange between the electrons leads to a broadening of the n-distribution. For im-

pact parameters less than ~ 15 μm the probability that one of the atoms is ionized becomes significant. The surviving atom transitions to a lower-lying Rydberg state with values of n centered near $n \sim 200$. Energy conservation within the electron subsystem suggests that the de-excited atoms should be in n states with $n < 306/\sqrt{2} \simeq 210$. Broadening of the atomic n-distributions during the initial approach of the Rydberg atoms leads to a corresponding broadening of the n-distribution of the de-excited atoms to higher $n > 210$. The broadening of the distribution to lower $n < 210$ reflects the energy distribution of the ionized electron.

The ionization cross section can be evaluated by integrating the ionization probability

$$\sigma_{\rm ion}\,(V) = \int_0^\infty 2\pi b P_{\rm ion}(b,V) db\,. \tag{3}$$

The cross section decreases with increasing velocity V (see Fig. 4). Around $V = 10$ m s^{-1} it reaches $\sigma_{\rm ion} \simeq 5\pi n^4$. We note that the calculated cross section for F states is $\sim 20\%$ larger than the values obtained using the full microcanonical ensemble [28], i.e., by averaging over all L states. This is consistent with the fact that the radius of the electronic wavefunction (or classically, the orbit), $\langle r\rangle = (3n^2 - L^2)/2$, is larger for values of $L/n \ll 1$. However, the difference is small and L changing due to interactions with other Rydberg atoms prior to an ionizing collision will only lead to small changes in the ionization cross section. At lower velocities, $V < V_A$, a further increase is observed in σ_{ion} which becomes proportional to $V^{-2/3}$ consistent with the velocity scaling of the ionization cross section predicted using the Langevin criterion [28]. However, as mentioned earlier quantum effects might modify the cross section in this low velocity regime and, therefore, the result is plotted with a dashed line.

B. Monte Carlo simulation for Rydberg-Rydberg collisions in the beam

The experimental data are analyzed using a Monte Carlo simulation of the formation and subsequent motion of an ensemble of Rydberg atoms created in a ground-state atom beam as it traverses the excitation volume. The details of the method are described in Ref. [25] and only a brief overview presented here. The atoms in the atom beam are initially distributed uniformly in space and their momentum distribution follows a sub-ensemble of a Maxwell-Boltzmann distribution with a beam divergence of $\theta_{\rm div} = 4$ mrad (i.e., $P_x/P > \cos(\theta_{\rm div}/2)$). The density of atoms is derived from the vapor pressure [31] in the oven. Since

the Rydberg-Rydberg interaction energies are much smaller than their kinetic energies (the beam temperature T is > 800 K), the atoms are assumed to travel with constant velocities. In the model it is assumed that, as ground-state atoms traverse the excitation volume, they are excited with a position-dependent excitation rate $\gamma(\vec{R})$. The distribution $\gamma(\vec{R})$ follows the intensity distribution associated with the crossed, focused laser beams and is approximated by a Gaussian distribution

$$\gamma(\vec{R}) = \gamma_0 \exp\left(-\frac{8X^2}{\Delta_X^2} - \frac{8Y^2}{\Delta_Y^2} - \frac{8Z^2}{\Delta_Z^2}\right), \tag{4}$$

where the focal point of the laser fields is at the origin, $\Delta_X = \Delta_Y = 50\mu$m is the $1/e^2$ diameter of the 767 nm laser and $\Delta_Z = 70$ μm is that of the 893 nm laser (the atom beam propagates along the X axis). The Rabi flopping period is much longer than the time (~ 120 ns) required for an atom to traverse the excitation volume allowing the excitation process to be treated perturbatively and characterized by a time-independent rate. The high density of states associated with the energy-shifted magnetic sublevels of a pair of F-state Rydberg atoms (multiplicity $(2L+1)^2 = 49$) results in a small, but finite, probability for excitation of multiple atoms within the blockade radius, R_B. We approximate this partial blockade by reducing the conditional excitation rate to $\Gamma(\vec{R}) \simeq 0.15\gamma(\vec{R})$ [25] when a Rydberg atom is already present within the blockade radius. The reduction factor 0.15 was determined through quantum calculations and the averaging of the excitation probabilities over all magnetic sublevels and the alignment of Rydberg atom pairs relative to the laser polarization. The present Monte Carlo simulation technique has been previously tested for short excitation pulses where collisions are unimportant [25]. Here we extend this method to include the effects of Rydberg-Rydberg collisions which become important for longer pulses. Accordingly we allow for ionization and de-excitation of Rydberg pairs when the atoms pass each other with velocity V at a distance $R < b_c(V) = \sqrt{\sigma_{\rm ion}(V)/\pi}$, where the ionization cross section $\sigma_{\rm ion}(V)$ is calculated from Eq. (3). For simplicity the simulation assumes that the de-excited atom does not ionize another Rydberg atom and plays no further role in any collisions. Additionally, the simulations indicate that modifications in quantum number n due to interaction with other Rydberg atoms are relatively small [Fig. 3(b)]. On the other hand, the variation in L can be quite large. But, as discussed above, the cross section is rather insensitive to the initial value of L and the effects of L-changing processes are also neglected.

The calculated distributions of interatomic spacings, impact parameters, and relative velocities in the ensembles of Rydberg atoms are shown in Fig. 5. The distributions are obtained by calculating for each Rydberg atom created the collision parameters relative to the "nearest" Rydberg atom where "nearest" does not refer to the smallest spatial separation but to the shortest time interval before a subsequent collision. To illustrate the effect of blockade on the kinematic collision parameters we first evaluate the mean values for the case of non-interacting atoms as a point of reference. A typical mean distance between Rydberg atoms (in the absence of blockade) is estimated to be $\bar{d} = P/(M\gamma_{\rm total}) \simeq 70$ μm from the average (ground-state) atom velocity P/M and the total excitation rate $\gamma_{\rm total} = \sum_{i=1}^{N_{\rm ex}} \gamma(\vec{R}_i) = 5.8 \times 10^6$ s^{-1} summed over the $N_{\rm ex}$ ground state atoms contained in the excitation volume. The corresponding nearest-neighbor distribution is shown in Fig. 5(a). As can also be seen in Fig. 5(a), the situation is very different for interacting atoms where the excitation of Rydberg atoms within the blockade radius, $R_B = 100\mu$m, is suppressed resulting in a nearest neighbor distribution that peaks at a value a little above 100 μm. The impact parameter distribution, however, is largely unaffected by blockade and is governed by the width of the laser beams transverse to the atomic beam propagation axis (Fig. 1). The distribution is peaked at a radius of ∼25-30 μm. The distribution of relative velocities for two atoms with a Maxwell-Boltzmann distribution is a Gaussian peaked at zero velocity. However, since the distribution shown in Fig. 5(c) does not include all Rydberg atom pairs but rather those with the shortest time interval before collisions, those pairs with small relative velocities (which take a long time to collide) are discriminated against and the distribution decreases to zero at $V = 0$. The relative velocity distribution of those atom pairs that collide [Fig. 5(c)] is therefore peaked around 170 m s^{-1} and their average relative velocity is estimated to be ~ 250 m s^{-1}, also marked in Fig. 4.

IV. TIME DEPENDENCE OF RYDBERG POPULATION

Figure 6 shows the time evolution of the average number of Rydberg atoms $\langle N_{\rm Ryd}\rangle$. The number of Rydberg atoms created can be estimated from $\langle N_{\rm meas}\rangle/\eta$ where the measured electron signal $\langle N_{\rm meas}\rangle$ is the average number of electrons detected following field ionization, both during and after, application of a 10μs-duration excitation pulse using the 893 nm IR laser powers indicated. For low IR laser powers (21 mW) the number of Rydberg atoms

formed is small, $\langle N_{\rm Ryd}\rangle \sim 1.5$, which points to creation of only one or two Rydberg atoms during the 10 μs excitation period. From the initial excitation rate (including a small but finite effect of blockade), the total Rydberg excitation rate $\gamma_{\rm total}$ at $R > R_B$ can be extracted analytically [25] yielding $\gamma_{\rm total} \sim 1.7 \times 10^5$ s^{-1}. Since the average ground-state strontium atom velocity P/M is $\sim$ 400 m s^{-1}, the mean distance between Rydberg atoms can be estimated to be $\bar{d} = P/(M\gamma_{\rm total}) \simeq 2.3$ mm which is much larger than the blockade radius ($\sim 100\mu$m). Therefore, the effect of blockade is negligible and, as might be expected, $\langle N_{\rm Ryd}\rangle$ increases linearly with time during the excitation pulse ($t < 10\mu$s). With an average relative velocity of $V \simeq 250$ m/s (see Fig. 5(c) the average collision rate is about $V/\bar{d} \simeq 10^5$ s^{-1}. However, given the distribution of impact parameters, only a small fraction of collisions lead to ionization and the collisional loss rate following the excitation pulse ($t > 10\mu$s), is expected to be small.

Use of higher IR laser powers [Fig. 6(b)] leads to increased Rydberg atom production. However, the values of $\langle N_{\rm Ryd}\rangle$ are less than would be expected were the Rydberg production rate simply proportional to IR laser power. Such scaling would suggest, for a laser power of 730 mW, a peak value of $\langle N_{\rm Ryd}\rangle$ of ~ 52 which is much larger than that observed. This deficit can be associated with the onset of strong blockade and collisional effects. In the absence of blockade effects, the mean distance between Rydberg atoms would be reduced to $\bar{d} \simeq 63\mu$m, significantly less than the blockade radius. When the blockade is taken into account, the production of Rydberg atoms with separations below the blockade radius R_B is suppressed and the distribution of separations peaks around $R_B \simeq 100$ μm (Fig. 5b). Correspondingly, the average collision rate is increased to $\sim 2.5 \times 10^6$ s^{-1} which increases the probability for collisional destruction. To further demonstrate the effects of blockade and collisions, values of $\langle N_{\rm Ryd}\rangle$ recorded when the oven temperature was increased from the normal operating value of $\sim$ 830 K to $\sim$ 890 K are included in Fig. 6(c). Whereas consideration of the strontium vapor pressure curves suggests that such a rise in temperature should increase the atomic beam density by a factor of $\sim$3.7, little increase in the Rydberg production rate is seen. (Only a limited number of measurements were possible at the highest oven temperature due to blocking of the apertures that collimate the strontium atom beam. Tight collimation is required to minimize the Doppler width of the transitions and enhance blockade.)

The results of the present simulations are shown in Fig.6 together with the measured values. For the 830 K atom beam the density of ground state atoms is estimated to be

3.2×10^8 cm^{-3}. The peak excitation rate for an IR laser power of 21 mW is set to $\gamma_0 = 1.2 \times 10^4$ s^{-1} so that the total rate $\gamma_{\rm total}$ matches the measured values at low intensities for which the effects of blockade and collisions are expected to be small. The model predictions agree well with the measured data (Fig. 6(a)). However, following the excitation pulse ($t > 10$ μs) the predicted decay of $\langle N_{\rm Ryd} \rangle$ is faster than predicted by the simulations. This discrepancy between experiment and theory can be attributed to Rydberg atom losses due to collisions with background gas and interactions with blackbody radiation which are not included in the present model. For the higher IR laser power, 730 mW, the excitation rate $\gamma_{\rm total}$ is increased and the effects of collisions are enhanced [Fig. 6(b)]. The model predictions are again in good agreement with experimental data. In modeling the data recorded at an indicated oven temperature of 890 K, the best fit is obtained by assuming a somewhat lower oven temperature of 855 K. This discrepancy might result from a small decrease in atomic beam density due to partial blocking of the beam defining apertures or because at a temperature of ~ 890 K the strontium vapor pressure in the oven is such that the collision mean free path is becoming comparable to the size of the exit aperture in the oven which results in changes in the aperture flow characteristics. Allowing for this, the model predictions are again in reasonable agreement with the measured results [Fig. 6(c)].

As a further test of the present model, measurements using Rydberg atoms with $n = 265$ were undertaken and revealed behavior similar to that seen at $n = 300$. Representative data obtained for $n = 265$ and a 10μs excitation pulse are presented in Fig. 7. Figure 7 also includes the results of calculations undertaken by appropriately scaling the parameters used in the model. The excitation rate scales as n^{-3} and for $n = 265$ is enhanced by a factor ~ 1.5 compared to that for $n = 300$. The blockade radius scales with $n^{11/6}$ [25] and is reduced to $\sim 80\mu$m. Therefore, the average number of Rydberg atoms detected, $\langle N_{\rm Ryd} \rangle \sim 35$, is larger than for $n = 300$. The ionization cross section $\sigma_{\rm ion}$ scales as n^4 and is reduced. As seen in Fig. 7, combining these scaling properties results in model predictions that agree well with experiment. This agreement further validates the model and the calculated blockade radii and collision cross sections that it uses as input.

V. CONCLUSIONS

The present work shows that the cross sections for the destruction of high-n atoms through collisions are large, 1-2 $\times 10^{-6}$ cm^2, and are comparable to those expected for "hard-sphere" collisions. The formation of a string-like ensemble of Rydberg atoms in a hot beam by exploiting the blockade effect provides unprecedented access to the study of destruction resulting from Rydberg-Rydberg collisions at high n, $n \simeq 300$, which must be taken into account when attempting to study other Rydberg-Rydberg interactions. Collisional destruction can be suppressed by production of Rydberg atoms in a cold gas although long-range attractive Rydberg-Rydberg interactions can still lead to collisions and eventual Rydberg atom destruction, albeit on longer time scales. Alternatively, collisional destruction can be suppressed in a hot beam if the excitation is localized to two, or more, (separately-blockaded) excitation volumes by, say, replacing the single 767 nm focused laser beam with multiple separate focused beams aligned along the axis of the 893 nm laser, and exciting only a single Rydberg atom in each focal spot. Multiple focal spots can be created, for example, by use of a Billet-type split lens or a spatial light modulator. Since the ground-state atom beam is tightly collimated, the product Rydberg atoms will travel parallel to each other thereby avoiding collisional ionization and facilitating study of their other longer-range interactions.

Acknowledgments

Research supported by the NSF under grant No. 1600059, the Robert A. Welch Foundation under Grant No. C-0734, by the FWF(Austria) (FWF-SFB041 ViCoM, and FWF-SFB049 NextLite). The Vienna scientific cluster was used for the calculations.

[1] D. Møller, L. B. Madsen, and K. Mølmer, Phys. Rev. Lett. **100**, 170504 (2008).

[2] T. Wilk, A. Gaëtan, C. Evellin, J. Wolters, Y. Miroshnychenko, P. Grangier, and A. Browaeys, Phys. Rev. Lett. **104**, 010502 (2010).

[3] X. L. Zhang, L. Isenhower, A. T. Gill, T. G. Walker, and M. Saffman, Phys. Rev. A **82**, 030306 (2010).

[4] D. Tong, S. M. Farooqi, J. Stanojevic, S. Krishnan, Y. P. Zhang, R. Côté, E. E. Eyler, and P. L. Gould, Phys. Rev. Lett. **93**, 063001 (2004).

[5] K. Singer, M. Reetz-Lamour, T. Amthor, L. G. Marcassa, and M. Weidemuller, Phys. Rev. Lett. **93**, 163001 (2004).

[6] E. Urban, T. A. Johnson, T. Henage, L. Isenhower, D. D. Yavuz, T. G. Walker, and M. Saffman, Nat. Phys. **5**, 110 (2009).

[7] A. M. Hankin, Y.-Y. Jau, L. P. Parazzoli, C. W. Chou, D. J. Armstrong, A. J. Landahl, and G. W. Biedermann, Phys. Rev. A **89**, 033416 (2014).

[8] D. Barredo, S. Ravets, H. Labuhn, L. Béguin, A. Vernier, F. Nogrette, T. Lahaye, and A. Browaeys, Phys. Rev. Lett. **112**, 183002 (2014).

[9] J. Deiglmayr, Phys. Scr. **91**, 104007 (2016).

[10] D. Jaksch, J. I. Cirac, P. Zoller, S. L. Rolston, R. Côté, and M. D. Lukin, Phys. Rev. Lett. **85**, 2208 (2000).

[11] M. Müller, I. Lesanovsky, H. Weimer, H. P. Büchler, and P. Zoller, Phys. Rev. Lett. **102**, 170502 (2009).

[12] L. Isenhower, E. Urban, X. L. Zhang, A. T. Gill, T. Henage, T. A. Johnson, T. G. Walker, and M. Saffman, Phys. Rev. Lett. **104**, 010503 (2010).

[13] S. E. Anderson, K. C. Younge, and G. Raithel, Phys. Rev. Lett. **107**, 263001 (2011).

[14] L. Li, Y. O. Dudin, and A. Kuzmich, Nature **498**, 466 (2013).

[15] J. E. Johnson and S. L. Rolston, Phys. Rev. A **82**, 033412 (2010).

[16] W. Li, P. J. Tanner, and T. F. Gallagher, Phys. Rev. Lett. **94**, 173001 (2005).

[17] T. Amthor, M. Reetz-Lamour, S. Westermann, J. Denskat, and M. Weidemüller, Phys. Rev. Lett. **98**, 023004 (2007).

[18] T. Amthor, M. Reetz-Lamour, C. Giese, and M. Weidemüller, Phys. Rev. A **76**, 054702 (2007).

[19] K. R. Overstreet, A. Schwettmann, J. Tallant, and J. P. Shaffer, Phys. Rev. A **76**, 011403 (2007).

[20] M. Viteau, A. Chotia, D. Comparat, D. A. Tate, T. F. Gallagher, and P. Pillet, Phys. Rev. A **78**, 040704 (2008).

[21] F. Robicheaux, J. Phys. B **38**, S333 (2005).

[22] Z. Feng, J. Miao, K. Zhao, D. Li, Z. Yang, F. Wu, Z. Wu, J. Zhao, and S. Jia, J. Phys. Soc. Jpn. **85**, 054301 (2016).

[23] M. Kiffner, D. Ceresoli, W. Li, and D. Jaksch, J. Phys. B **49**, 204004 (2016).

[24] X. Zhang, F. B. Dunning, S. Yoshida, and J. Burgdörfer, Phys. Rev. A **92**, 051402 (2015).

[25] S. Yoshida, J. Burgdörfer, X. Zhang, and F. B. Dunning, Phys. Rev. A **95**, 042705 (2017).

[26] A. N. Klucharev and V. Vujnović, Phys. Rep. **185**, 55 (1990), ISSN 0370-1573.

[27] A. Reinhard, T. Cubel Liebisch, K. C. Younge, P. R. Berman, and G. Raithel, Phys. Rev. Lett. **100**, 123007 (2008).

[28] R. E. Olson, Phys. Rev. Lett. **43**, 126 (1979).

[29] A. Müller, N. Djuric, G. H. Dunn, and D. S. Belić, Rev. Sci. Instrum. **57**, 349 (1986).

[30] R. Abrines and I. C. Percival, Proc. Phys. Soc. **88**, 861 (1966).

[31] G. D. Maria and V. Piacente, J. Chem. Therm. **6**, 1 (1974).

Figures

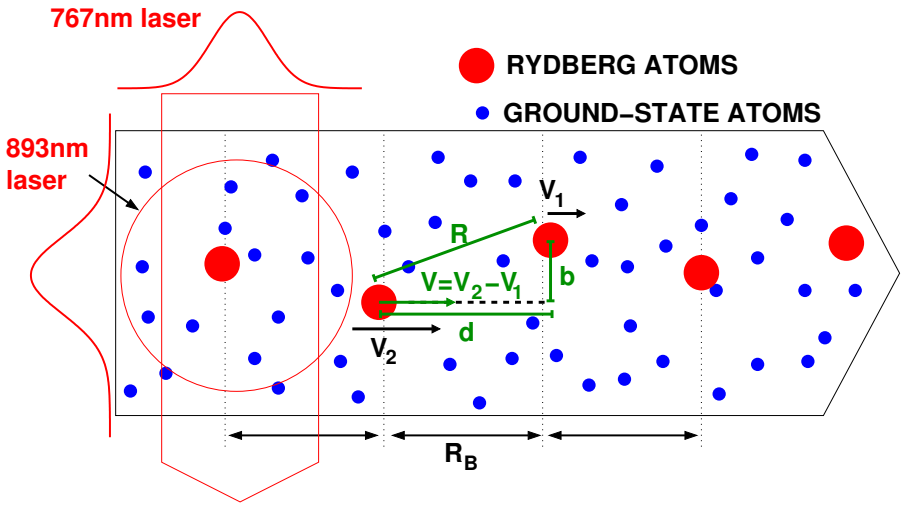

FIG. 1: Schematic drawing of Rydberg formation in the atomic beam. Initially the atoms are in the ground state and a small number of them are excited to Rydberg states by the overlapped laser beams. Rydberg blockade leads to formation of a string-like ensemble of Rydberg atoms with a mean spacing $\bar{d}$ along the beam direction of the order of the blockade radius. The transverse distribution is controlled by the laser intensity profile. The kinematic parameters used in analyzing the collisions, i.e., the interatomic spacing R, the impact parameter b, and the relative velocity V) are also indicated.

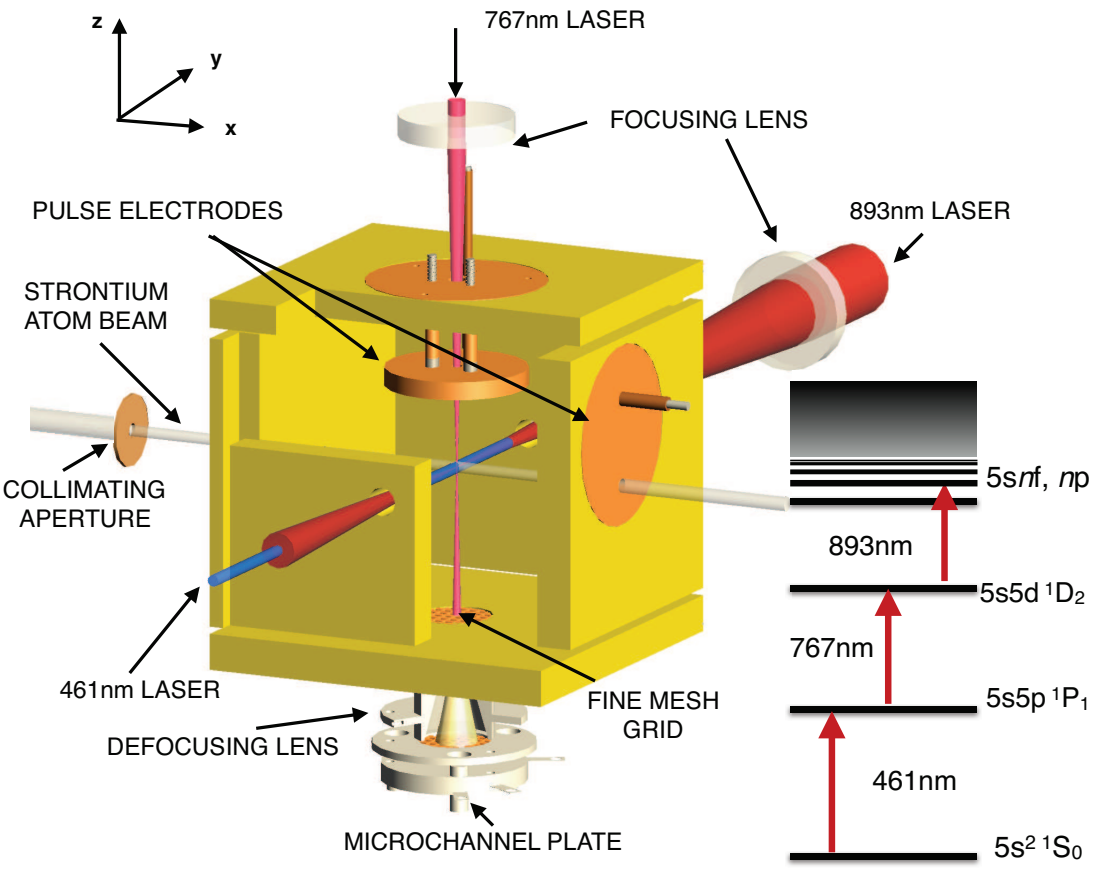

FIG. 2: Schematic diagram of the apparatus. The inset shows the excitation scheme employed.

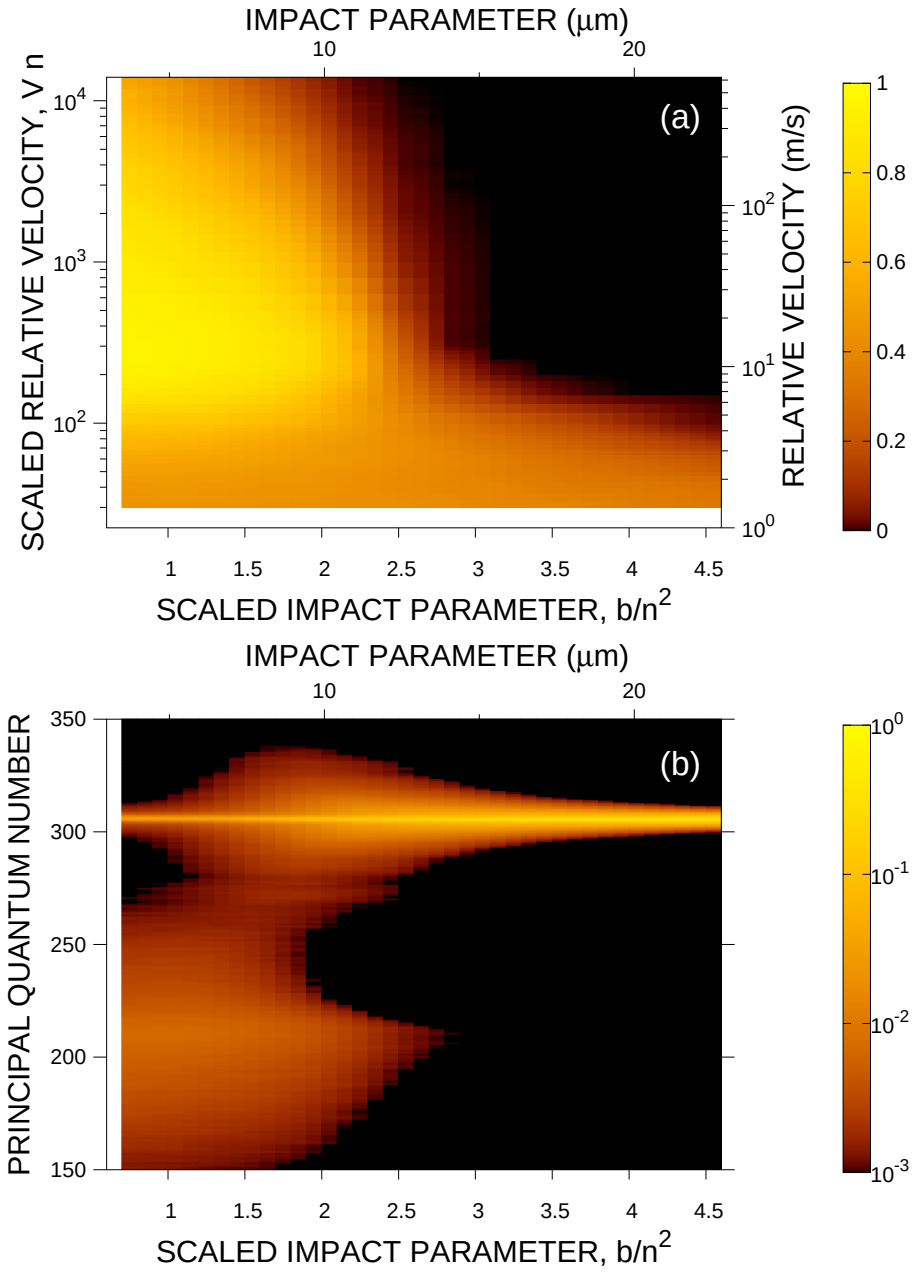

FIG. 3: (a) Calculated ionization probability for a collision of two Rydberg atoms as a function of impact parameter b and initial velocity. (b) The n-distribution after collisions plotted as a function of impact parameter. The electronic state of the Rydberg atoms is approximated by a sub-ensemble of a microcanonical ensemble with $n = 306$ and $L = 3$ (see text). The initial separation between the atoms is set to $R = 30n^2 \simeq 150\mu$m.

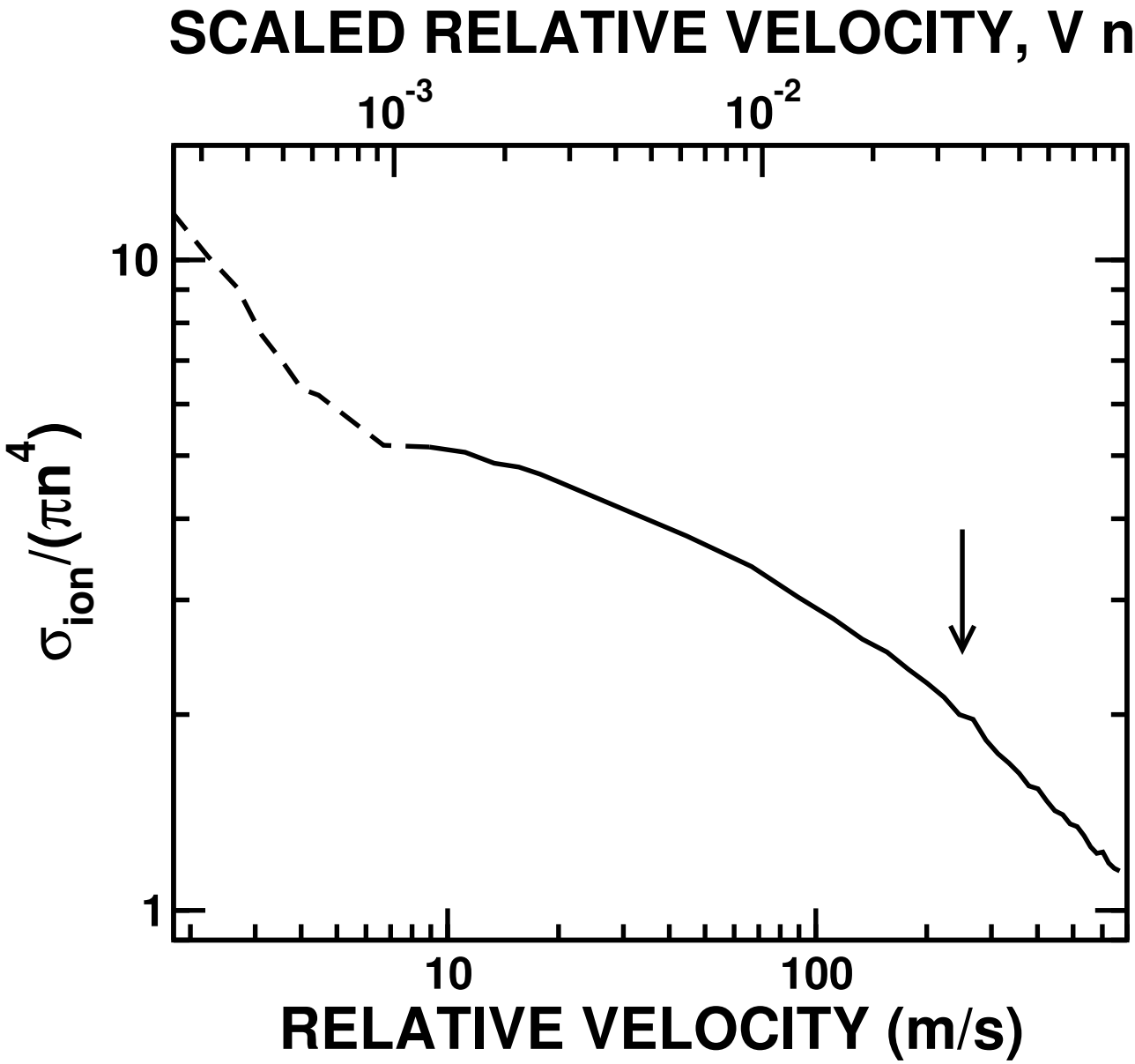

FIG. 4: Cross section, $\sigma_{\rm ion}(V)$, for ionization in a collision of two Rydberg atoms in the initial state $n = 306$ and $L = 3$ as a function of initial relative velocity v. The arrow indicates the average relative velocity (~ 250 m/s) for the 830 K atomic beam. The cross section is plotted in units of $\pi n^4 \simeq 25\pi(\mu\mathrm{m})^2$.

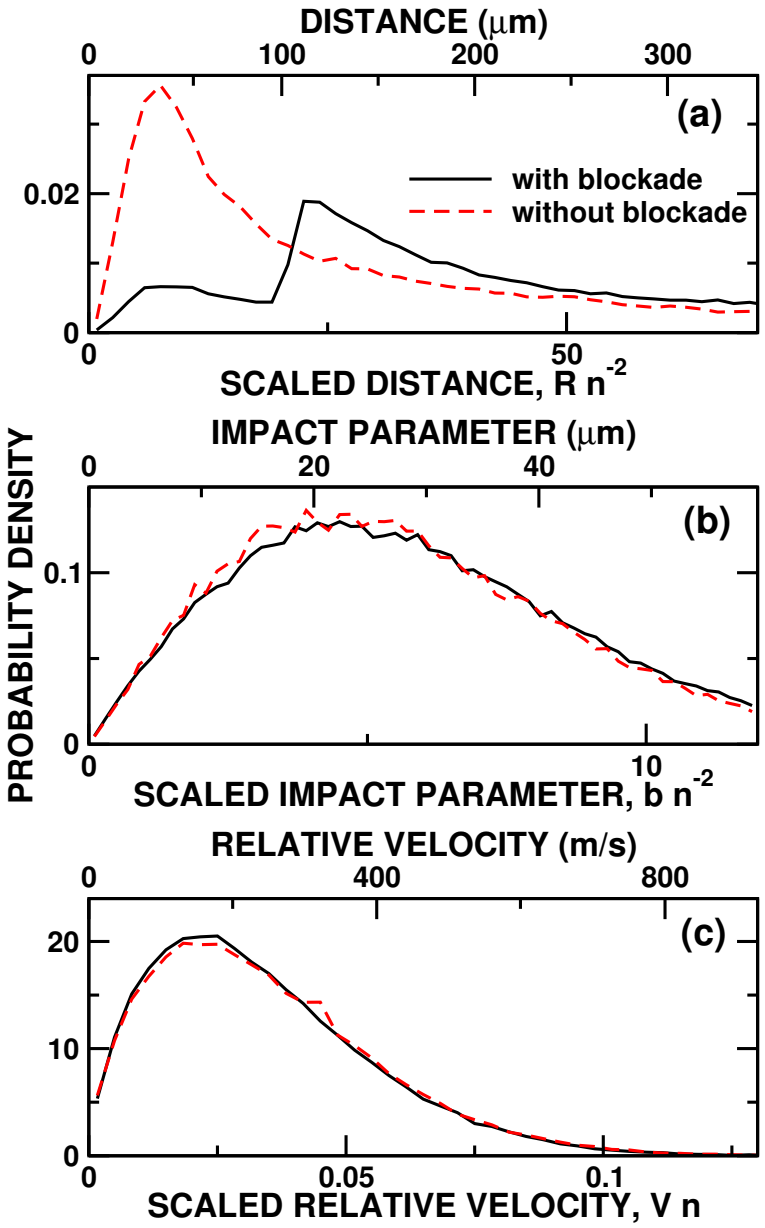

FIG. 5: Calculated probability distributions for (a) the distance, (b) the impact parameter, and (c) the relative velocity, between Rydberg atoms. The solid lines are the distributions for interacting atoms and the dashed lines for non-interacting atoms. These parameters are evaluated for pairs of Rydberg atoms with the shortest time to the next collision. The parameters used to derive these distributions are taken from the experimental conditions, i.e., an atom beam temperature of 830 K and a laser power of 730 mW.

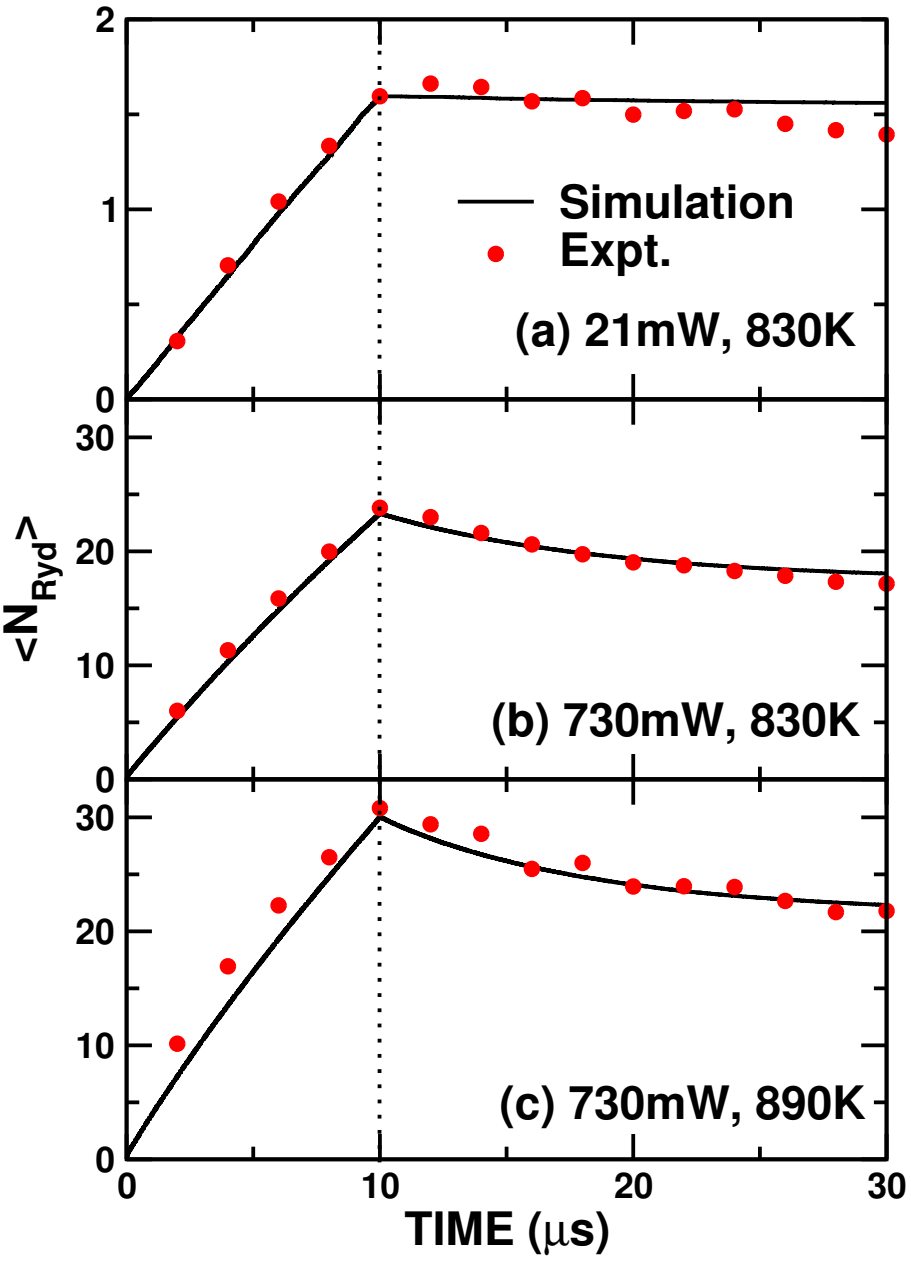

FIG. 6: Measured and calculated time development of the Rydberg populations. The measured data (symbols) are corrected for the detection efficiency, $\eta = 0.3$. The calculations use a blockade radius of 100μm and the ionization cross section $\sigma_{\rm ion}(v)$ shown in Fig. 4. The total excitation rate $\gamma_{\rm total} = 1.2 \times 10^4 {\rm s}^{-1}$ at a laser power of 21 mW is extracted from the measurements in (a). For (b) and (c) the excitation rate is scaled according to the laser intensity and the atom beam density. The simulation for the 890K data assumes an oven temperature of 855K (see text). The dashed line indicates the conclusion of the excitation pulse.

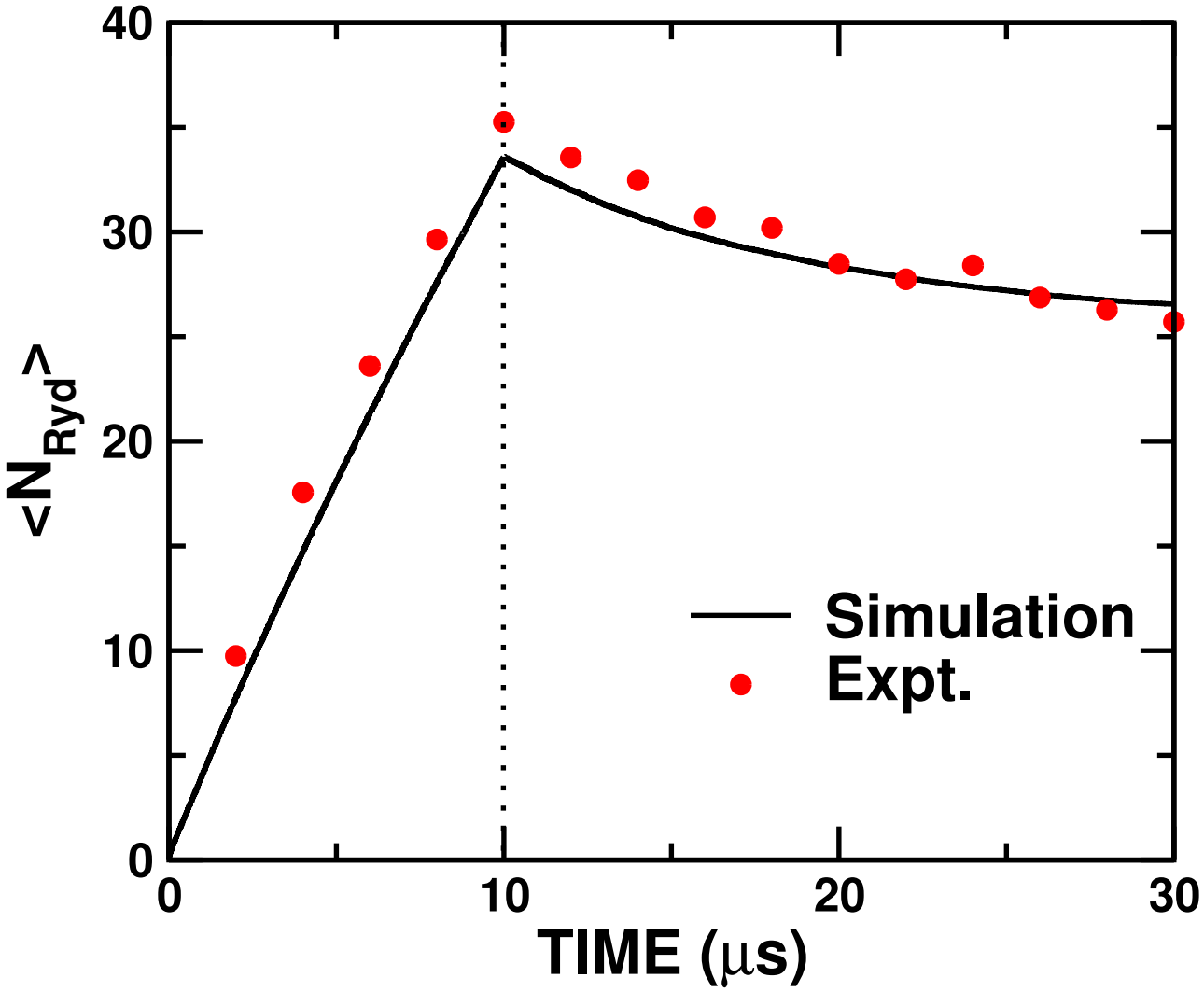

FIG. 7: Time evolution of the measured and calculated average number of $n = 265$ Rydberg atoms, $\langle N_{\rm Ryd}\rangle$, during and after application of a 10μs-duration excitation pulse with an IR laser power of 730 mW and an oven temperature of 830 K. The measured data are corrected for the detection efficiency, $\eta = 0.3$. The calculation employs parameters scaled from those used for $n = 300$: total excitation rate $\gamma_{\rm total} \simeq 8.4 \times 10^6$ s^{-1}, blockade radius $R_B \simeq 80\mu$m, and impact parameter $\sigma_{\rm ion}(v)(265/300)^4$. The dashed line indicates the end of the excitation pulse.